Synthetic Metals 210 (2015) 288–296

Contents lists available at ScienceDirect

Synthetic Metals

journal homepage: www.elsevier.com/locate/synmet

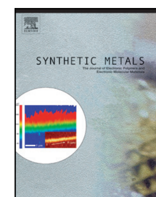

Logarithmic organic photodetectors

Elsayed Elgazzar[a], Mehmet Ozdemir[b], Hakan Usta[b], Ahmed A. Al-Ghamdi[c], A. Dere[d], Farid El-Tantawy[a], F. Yakuphanoglu[c,d,e,*]

[a] Department of Physics, Faculty of Science, Suez Canal University, Ismailia, Egypt
[b] Department of Materials Science and Nanotechnology Engineering, Abdullah Gül University, Kayseri, Turkey
[c] Physics Department, Faculty of Science, King Abdulaziz University, Jeddah, Saudi Arabia
[d] Department of Physics, Faculty of Science, Fırat University, Elazig, Turkey
[e] Nanoscience and Nanotechnology Laboratory, Fırat University, Elazig, Turkey

ARTICLE INFO

Article history:
Received 12 September 2015
Received in revised form 6 October 2015
Accepted 11 October 2015
Available online 12 November 2015

Keywords:
Graphene oxide
Organic semiconductor
Photodiode

ABSTRACT

A novel photodetector of Al/GO:C8-BTBT/n-Si/Au with various graphene oxide (GO) contents has been investigated. The electrical properties of the diodes were characterized by current–voltage (*I*–*V*) and capacitance–voltage (*C*–*V*) measurements. The values of barrier height, ideality factor, and series resistance of the diodes were determined from *I*–*V* characteristic curves by using Norde's equations. The photocurrent properties of the diode were studied under various illumination intensities. The photoconducting mechanism of the diodes is controlled by the traps. The photoresponse properties of the diodes are increased with GO contents. The obtained results indicate that graphene oxide doped 2,7-dioctyl[1]benzothieno[3,2-b][1]benzothiophene/n-Si heterojunctions can be used as a photodetector for optoelectronic applications.

© 2015 Elsevier B.V. All rights reserved.

1. Introduction

Organic semiconductor-based optoelectronic devices have attracted a great deal of attention in the field of semiconductors and optoelectronics. These devices have several advantages such as low-cost, flexibility, and facile structure/device modification, and they can be fabricated on various plastic and inorganic substrates at room temperature by using solution processing techniques [1]. In addition, unique optical and electrical properties can be obtained with organic materials compared to inorganic-based semiconductors [2–13]. Recently, a series of π-extended heteroarene semiconductors including [1]benzothieno[3,2-b][1]benzothiophene (BTBT), dinaphtho[2,3-b:20,30-f]thieno[3,2-b]thiophene (DNTT), and dianthra-[2,3-b:20,30-f]thieno[3,2-b]thiophene (DATT) have been developed based on fused aromatic units, and charge carrier mobilities exceeding those of amorphous silicon (0.5–1 $cm^2/V s$) have been achieved. [14]. Specifically, solution-processable p-type semiconductor, 2,7-dioctyl[1]benzothieno[3,2-b][1]benzothiophene (C8-BTBT) (Fig. 1), has shown impressive hole mobilities up to 25 $cm^2/V \cdot s$, which is one of the highest results achieved in organic semiconductor materials [14]. Organic/inorganic multi-layered hybrid devices have recently attracted great attention, which has been facilitated by the availability of various organic semiconducting materials [11–14]. In these devices, organic/inorganic heterojunctions play key roles in controlling the device operation and performance, and the rational integration of high performance organic materials in these devices may significantly enhance their optoelectronic characteristics. Over the past decade, graphene oxide (GO) has attracted widespread attention because of its remarkable properties such as superior mechanical strength [15], excellent charge carrier mobility [16], high thermal conductivity [17], and large specific surface area [18,19].

The motivation in the present work is to study photodiodes of Al/C8-BTBT/n-Si/Au based on a p-type small molecule semiconductor, [1] benzothieno[3,2-b][1]benzo-thiophene (C8-BTBT), and to investigate the effect of graphene oxide doping in Al/C8-BTBT:GO/n-Si/Au diode structure for low-cost, high-performance optical sensing applications.

2. Experimental details

All reagents were purchased from commercial sources and used without further purification unless otherwise noted. Conventional

* Corresponding author at: Nanoscience and Nanotechnology Laboratory, Fırat University, Elazig, Turkey. Fax:+90 424 2330062.
E-mail address: fyhan@hotmail.com (F. Yakuphanoglu).

http://dx.doi.org/10.1016/j.synthmet.2015.10.008
0379-6779/© 2015 Elsevier B.V. All rights reserved.

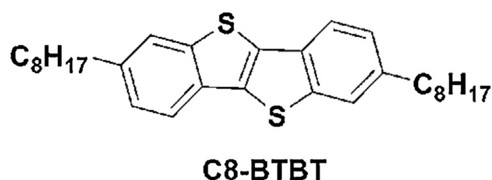

Fig. 1. Chemical structure of 2,7-dioctyl[1]benzothieno[3,2-b][1]benzothiophene (C8-BTBT).

Schlenk techniques were used, and reactions were carried out under N_2 unless otherwise noted. NMR spectra were recorded on a Bruker 400 spectrometer (^{1}H, 400 MHz and ^{13}C, 100 MHz). Elemental analyses were performed by ERU-Technology Research and Application Center on LECO/TruSpec Micro-Elemental Analysis Instrument.

Sythesis and characterization

The synthetic route to C8-BTBT is shown in Scheme 1. The synthesis of Benzothieno[3,2-b][1]benzothiophene (BTBT, **1**) was performed according to the reported procedure [20].

Synthesis of ([1]benzothienopheno[3,2-b]benzothienophene-2,7-diyl) bis(octan-1-one) (2)

To a solution of [1] benzothieno[3,2-b][1]benzothiophene (1.0 g, 4.16 mmol) in 50 mL of anhydrous dichloromethane, $AlCl_3$ (3.07 g, 23 mmol) was added at −10 °C under nitrogen. The resulting mixture was stirred at −10 °C for 30 min, and then octanoylchloride (3.41 g, 21 mmol) was added dropwise. The reaction mixture was stirred at −10 °C for 1 h, and then at room temperature for 2 days. The reaction mixture was poured into water to yield a white precipitate. The precipitate was collected by vacuum filtration, and washed with water and methanol, respectively, to give **2** (1.3 g, 64% yield) as a white crystalline solid. This compound was directly used in the next step without any further purification. ^{1}H NMR δ 8.56 (d, J = 1.3 Hz, 2H), 8.06 (dd, J = 8.0, 1.3 Hz, 2H), 7.95 (d, J = 8.0 Hz, 2H), 3.07 (t, J = 7.0 Hz, 4H), 1.75–1.83 (m, 4H), 1.20–1.52 (m,16H), 0.90 (t, J = 7.2 Hz, 6H).

Synthesis of 2,7-dioctyl[1]benzothieno[3,2-b][1]benzothiophene (C8-BTBT)

To a solution of ([1]benzothienopheno[3,2-b]benzothienophene-2,7-diyl) bis(octan-1-one) (2, 1.0 g, 2.03 mmol) and potassium hydroxide (626 mg, 11.2 mmol) in diethyleneglycol (50 mL) was added hydrazine hydrate (3.2 mL, 51.75 mmol) under nitrogen, and the resulting solution was heated to 110 °C for 1 h and then further heated at 210 °C for 5 h. After cooling to room temperature, a white precipitate formed, which was filtered and washed with water and methanol to yield a white crude solid. The crude compound was next chromatographed on silica, eluting with hexanes to yield C8-BTBT as a white crystalline solid (0.66 g, 70% yield). ^{1}H NMR δ 7.76 (d, J = 8.0 Hz, 2H), 7.71 (d, J = 1.0 Hz, 2H), 7.27 (dd, J = 8.0 Hz,1.0 Hz, 2H), 2.76 (t, J = 8.0 Hz, 4H), 1.71 (m, 4H), 1.26–1.36 (m, 20H), 0.89 (t, J = 6.8 Hz, 6H); ^{13}C NMR δ 143.2, 140.5, 132.7, 131.1, 124.9, 122.9, 121.2, 36.2, 31.9, 32.0, 29.2, 29.1, 28.8, 22.5, 13.9; Anal. Calc. for $C_{30}H_{40}S_2$: C, 77.53; H, 8.67. Found: C, 77.20; H, 8.50.

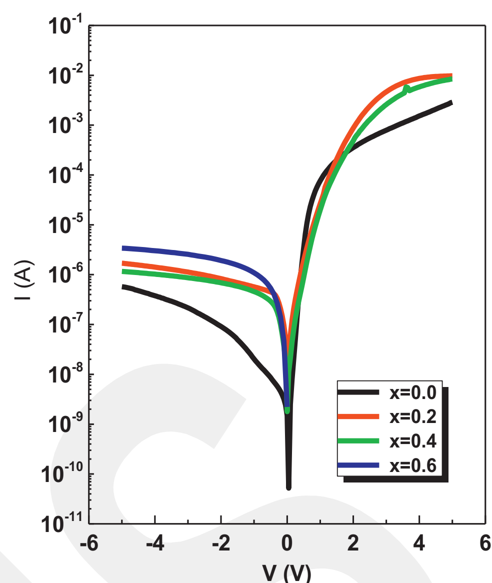

Fig. 2. Dark *I–V* characteristics of Al/GO:C8-BTBT/n-Si/Au diode with for various *x* contents (*x* = GO:C8-BTBT)

Firstly, graphene oxide was prepared by Hummer's method. The C8-BTBT was dissolved in dichlorobenzeneand GO was ultrasonically dispersed in chloroform for 2 h. The composites were prepared using C8-BTBT and GO solutions for various weight ratios of (*x* = GO:C8-BTBT) (*x* = 0.0, 0.2, 0.4 and 0.6). The C8-BTBT and GO solutions were coated onto surface of n-Si substrate using drop casting method. Before coating procedure, the silicon substrates were was etched by HF and then rinsed in deionized water using an ultrasonic bath for 10–15 min. The silicon wafers were chemically cleaned with methanol and acetone baths, respectively. Top contact of the diodes was prepared by Au metal. For this, Au metal was evaporated by sputtering system in the form of circles giving a diode contact area of 3.14×10^{-2} cm^2. Surface morphology of the films was investigated using a scanning electron microscopy (SEM). The current–voltage (*I–V*) characteristics of the diodes were performed using a KEITHLEY 4200 semiconductor characterization system (SCS). Photoresponse measurements were performed using a solar simulator and KEITHLEY 4200 SCS. The intensity of the illumination was measured using a solar power meter (TM-206).

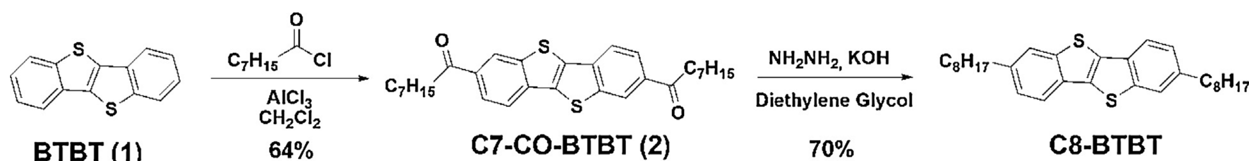

Scheme 1. Synthetic route to C8-BTBT.

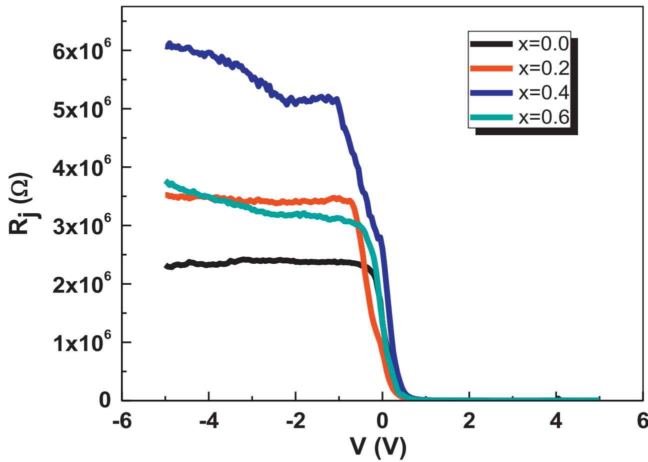

Fig. 3. Plots of R_j vs. V of Al/GO:C8-BTBT/n-Si/Au diodes for various x contents.

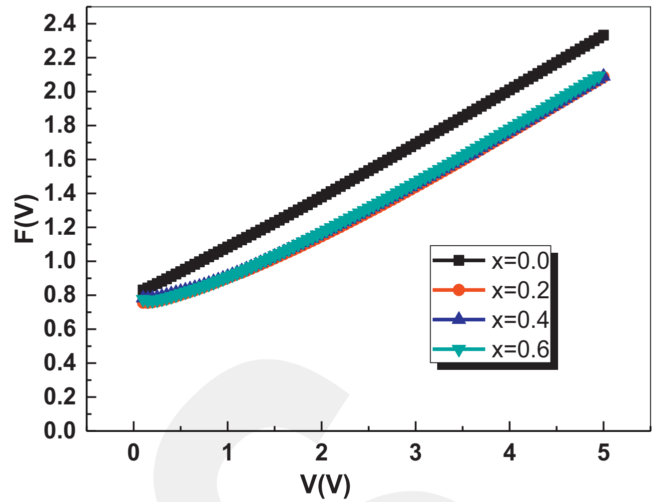

Fig. 4. F(V) vs. V plots of Al/GO:C8-BTBT/n-Si/Au diodes in dark for various x values.

3. Result and discussions

3.1. Current–voltage characteristics of the diodes

The current–voltage (I–V) characteristics of Al/GO:C8-BTBT/n-Si/Au diodes under dark conditions at room temperature are shown in Fig. 2. It is observed that the current is increased with GO contents, and the diodes show a rectifying behavior. The current–voltage characteristics of the fabricated diode can be analyzed by the following thermionic emission theory [21–23]:

$$I = I_o \exp\left(\frac{q(V-IR)}{nkT}\right)\left[1-\exp\left(-\frac{q(V-IR_s)}{kT}\right)\right] \quad (1)$$

where V is the applied voltage, q is the electronic charge, n is the ideality factor, k is the Boltzmann constant, T is the absolute temperature, R_s is the series resistance and I_0 is the saturation current [23].

When the non-ideal Schottky barrier diode with a series resistance and an interfacial layer are considered, it is assumed that the net current of the device is due to thermionic emission theory and it can be expressed by the following relation [23,24]:

$$I = I_o\left[\exp\left(\frac{q(V-IR_s)}{nkT}\right)-1\right] \quad (2)$$

where

$$I_0 = AA^*T^2\exp\left(\frac{-q\phi_b}{kT}\right) \quad (3)$$

is the saturation current,ϕ_b is the zero bias effective barrier height, $A^*$is the effective Richardson's constant which equals (112 Acm^{-2}K^{-2}for n-type silicon) and A is the effective diode area [25,26]. The slope and the intercept of the forward bias plot of In (I) vs. voltage (V) yield the values of ideality factor, n and barrier heightϕ_b, respectively. Al/GO:C8-BTBT/n-Si/Au heterojunction diode with values of ideality factor n greater than unity, exhibits a non-ideal behavior. This is mainly due to the high values of ideality factor, which results in the existence of Schottky barrier height inhomogeneity, presence of interfacial states and series resistance [27]. I–V behavior of the diode is affected by series resistance R_s and shunt resistanceR_{sh}, which are related to the interfaces of semiconductor–semiconductor and semiconductor–electrode, respectively [28]. It is well known that ideal device requires low series resistance and high shunt resistance.

As shown in Fig. 3, the junction resistance R_j of the diode can be determined using dark current–voltage characteristics expressed as [27]:

$$R_j = \frac{\partial V}{\partial I} \quad (4)$$

Schottky diode parameters (n, ϕ_b, R_s and R_{sh})of Al/GO:C8-BTBT/n-Si/Au diode with different GO contents were calculated and presented in Table 1. Barrier height and series resistance of the device can also be achieved using a method developed by Norde as shown in Fig. 4 from the following function [29,30]:

$$F(V) = \frac{V}{\gamma} - \frac{kT}{q}\ln\left(\frac{I(V)}{AA^*T^2}\right) \quad (5)$$

where, γ is the first integer greater than ideality factor. I(V) is the current obtained from the I–V curve. Once the minimum of the F(V) vs. V plot is determined from Fig. 4, the value of barrier height can be obtained from Eq. (6), where F(V) is the minimum point of F(V) and V_o is the corresponding voltage.

$$\phi_b = F(V) + \frac{V_o}{\gamma} - \frac{kT}{q} \quad (6)$$

The series resistance of the junctions can be calculated as follows [31]:

$$R_s = \frac{kT(\gamma-n)}{qI(V_o)} \quad (7)$$

Table 1
Electrical parameters obtained from I–V characteristics and Norde equation for Al/GO:C8-BTBT/n-Si/Au Schottky diode with various x ratios.

x	I–V characteristics				Norde equation	
	n	ϕ_b	R_s (Ω)	$R_{sh} \times 10^6$ (Ω)	R_s (Ω)	ϕ_b (V)
0.0	1.68	0.891	4619	2.4	1.1×10^4	0.87
0.2	2.53	0.787	1442	3.4	8.57×10^3	0.78
0.4	2.45	0.797	2575	5.3	1.40×10^3	0.87
0.6	2.56	0.812	2239	3.2	2.21×10^3	0.80

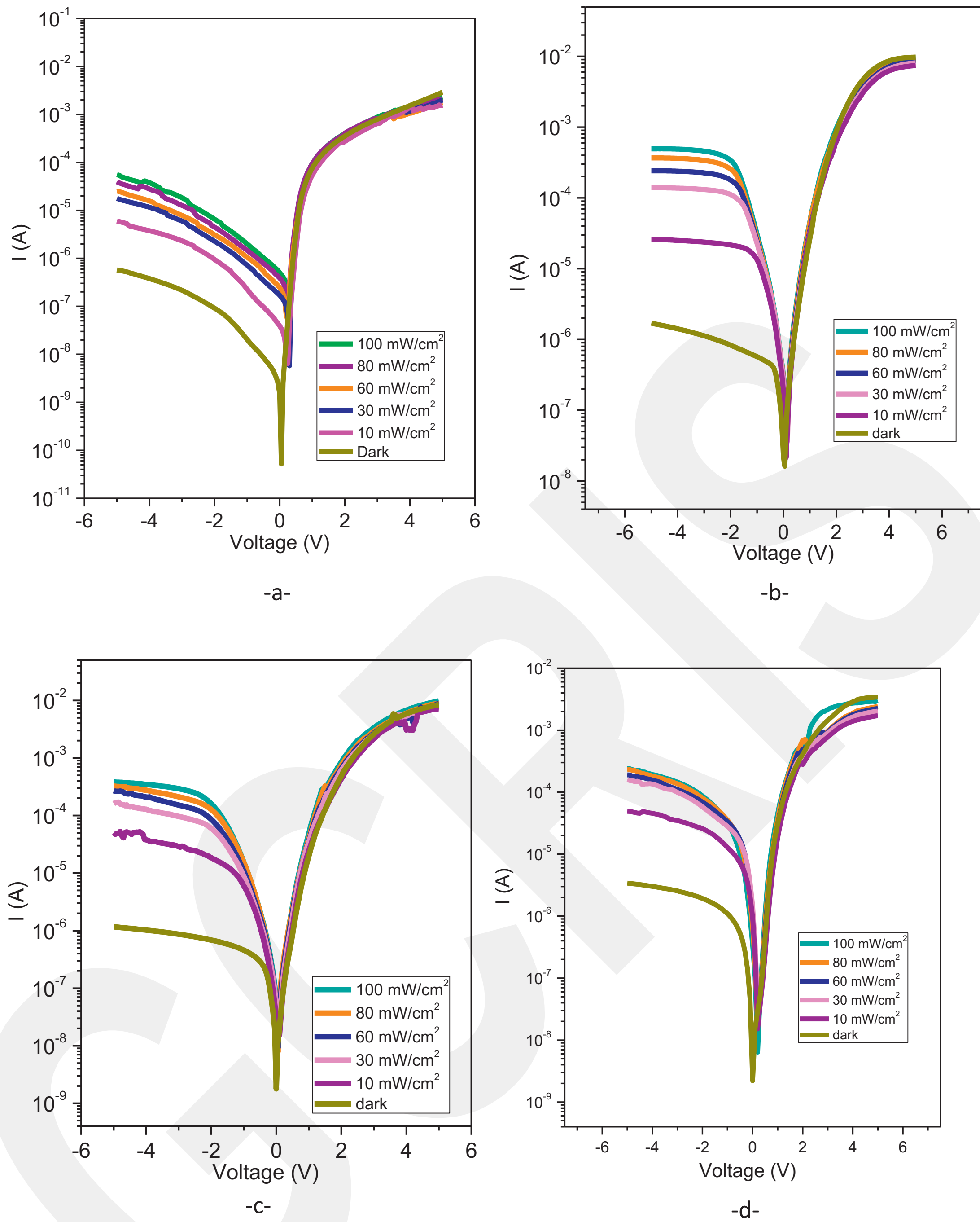

Fig. 5. *I*–*V* plots of Al/GO:C8-BTBT/n-Si/Au diode under different illuminations (a) $x = 0.0$ (b) $x = 0.2$ (c) $x = 0.4$ (d) $x = 0.6$

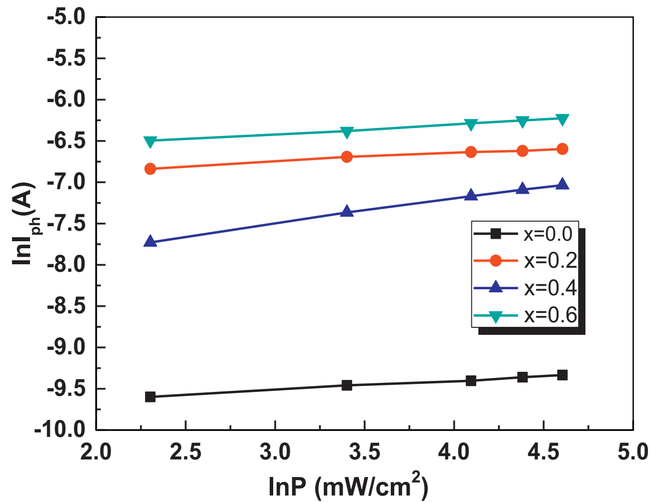

Fig. 6. Variation of the photocurrent with light intensity of Al/GO:C8-BTBT/n-Si/Au diodes

where I is the corresponding current. The photodiode parameters were calculated and presented in Table 1.

3.2. Photocurrent and photoresponse properties of the diodes

The photo-response properties of Al/GO:C8-BTBT/n-Si/Au diodes under various illuminations are shown in Fig. 5(a and d). It is clearly evident that the current increases strongly with light illumination. The diode exhibits a good photo-response behavior with low open circuit voltage, low short circuit current and high photocurrent values, confirming its excellent photocurrent response to light intensity. On the other hand, it is clear that the photodiode current increases with GO dopant.

Photocurrent dependence of light intensity is expressed by the following relation [32,33]:

$$I_{Ph} = AP^{m} \tag{8}$$

where I_{Ph} is the photocurrent, A is a constant, P is the illumination intensity and m is an exponent.Eq. (8) applies only in photoconductive mode for the diodes. The constant m was determined from the slope of $\log(I_{Ph})$ versus $\log(P)$ plot as shown in Fig. 6. The obtained m values of the diodes with various GO contents were 0.112 (x = 0.0), 0.103 (x = 0.2), 0.302 (x = 0.4), and 0.118 (x = 0.6). It is noteworthy that the value of m indicates the presence of the trap centers within the band-gap, and in our diode system, after x = 0.4 content, it becomes three times higher than its GO-undoped value. The photoconducting mechanism of the diode is governed by the traps, which confirm the enhancement of the diode performance by doping with GO.

For further photoresponse analysis, the transient photocurrent measurements of the diodes prepared with x = 0.2 and x = 0.6 ratios were performed as shown in Fig. 7(a and d). In the on-state, the current of the diode rapidly increases to a certain level and then gradually saturates to its maximum value. After turning off, the current comes back to its initial state. When the diode was illuminated, the number of photogenerated charge carries increased with the illumination and the electrons contribute to the current. After turning off the light, the number of free electrons is decreased and the current of the diode decreases. The photoconducting properties of the diode depend on the trap centers present in the diode. It was observed that the photodiode current logarithmically increases with illumination intensity.

3.3. Capacitance–voltage and conductance–voltage characteristics of Al/GO:C8-BTBT/n-Si/Au diodes

Fig. 8(a–d) shows the variation of capacitance and conductance with frequency at different bias voltages for undoped diode structure of Al/GO:C8-BTBT/n-Si/Au.

The effect of series resistance on the capacitance and conductance were corrected by using the corrected capacitance (C_{adj}) and corrected conductance (G_{adj}) [35–36].

$$C_{adj} = \frac{\left[G_m^2 + (\omega C_m)^2\right] C_m}{a^2 + (\omega C_m)^2} \tag{9}$$

$$G_{adj} = \frac{\left[G_m^2 + (\omega C_m)^2\right] a}{a^2 + (\omega C_m)^2} \tag{10}$$

$$a = G_m - \left[G_m^2 + (\omega C_m)^2\right] R_s \tag{11}$$

where C_{adj} is the corrected capacitance, G_{adj} is the corrected conductance. The decrease in the capacitance at high frequencies depends on the ability of the charge carriers to follow the applied alternating current (AC) signal [34,35]. It can be observed that there are shifts in the peak of the curves of C–V with different frequencies, which may be due to the existence of interface states. This behavior could be explained on the basis of the presence of a continuous distribution of the interface states in the interface of the diode [36,37]. The response of the interface states is changed with the frequency of applied alternating voltage and this causes a decrease in capacitance, as the charges at the interface states can follow the alternating current signal at lower frequencies.The conductance–voltage (G–V) measurements at different frequency are shown in Fig. 8(c and d). It is observed that, G and G_{adj} of the diode is dependent on the voltage and frequency in the forward bias voltage while the conductance in the reverse bias voltage is remain constant with change in frequency. The value of R_s for the diode was calculated using conductance method developed by Nicollian and Goetzberger [38,39].

$$R_s = \frac{G_m}{G_m^2 + (\omega C_m)^2} \tag{12}$$

where, C_m and G_m are the measured capacitance and conductance, respectively. Fig. 9 shows the variation of series resistance for undoped photodiode with applied voltage and frequency. It was observed that the series resistance was high at low frequency and decreases with increasing frequency.

The high value of series resistance at low frequencies is because the interface states can follow the AC signal and yield an excess capacitance at low frequency. We also observed a peak in the series resistance vs. voltage plot. The peak position depends on the applied frequency which could be due to the fact that interface charges depend on the applied frequency [40–43]. As seen from Fig. 10(a–d) the capacitance decrease and conductance increase with high frequencies for Al/GO:C8-BTBT/n-Si/Au diode with 6 mg GO contents. Moreover, the conductance–voltage plots of the diode with x = 0.6 give a high conductance compared to those with undoped GO contents.

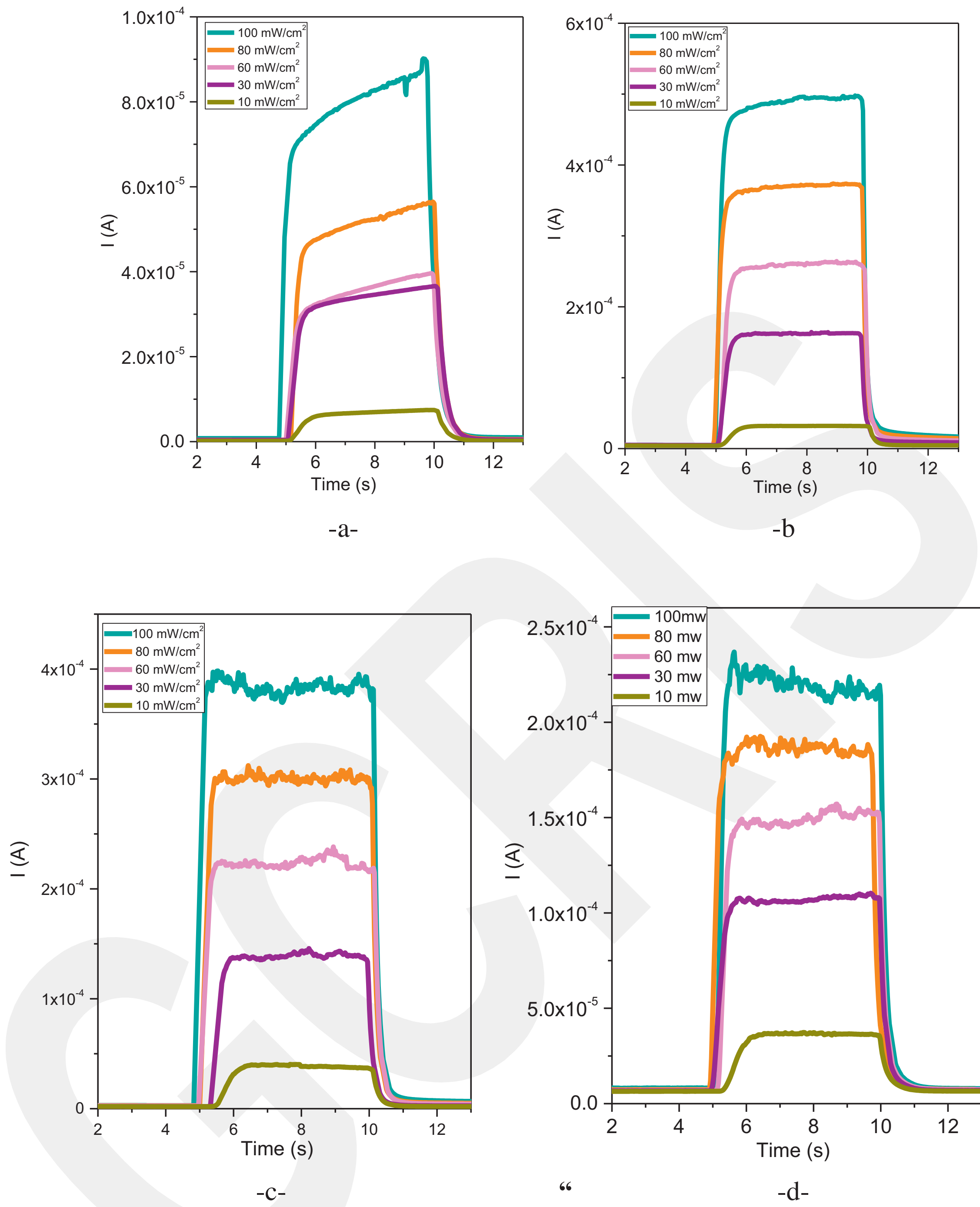

Fig. 7. Phototransient current plots of Al/GO:C8-BTBT/n-Si/Au diodes (a) $x = 0.0$ (b) $x = 0.2$ (c) $x = 0.4$ (d) $x = 0.6$

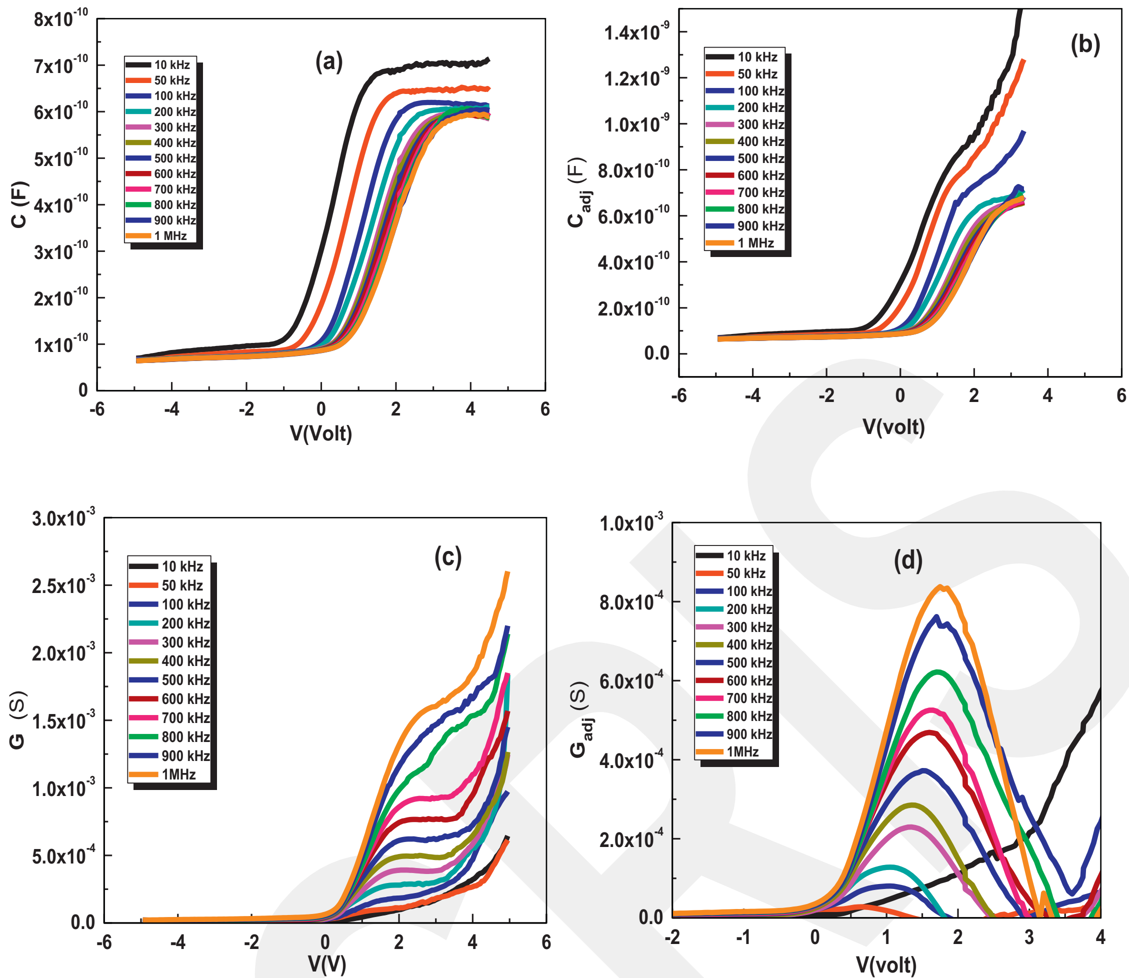

Fig. 8. *C–V* (a), C_{adj}–*V* (b), *G–V* (c) and G_{adj}–*V* (d) characteristics of Al/GO:C8-BTBT/n-Si/Au diode at various frequencies.

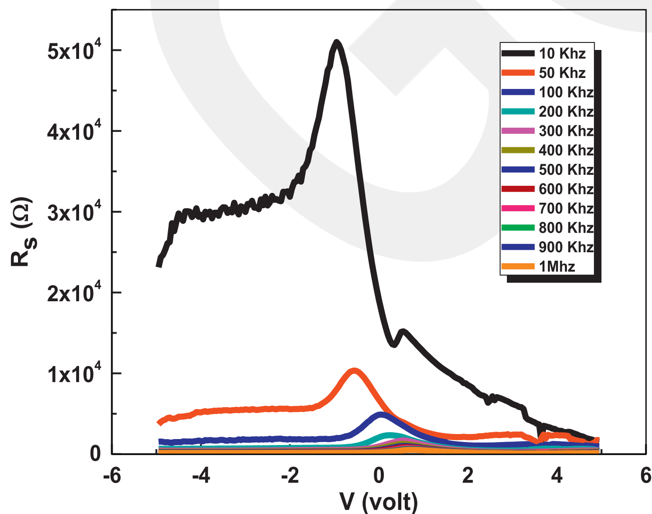

Fig. 9. R_s–*V* characteristics of Al/GO:C8-BTBT/n-Si/Au diode at various frequencies.

The frequency dependence of series resistance–voltage (R_s–V) plots of diode with x=0.6 is given in Fig. 11. As seen in Fig. 11, the value of R_s decreases with increasing frequency. On the other hand, R_s–V plots of diode at 10 kHz give two peaks at about 0.95 and −0.55 volt while R_s–V plots of diode with undoped GO content give two peaks at about 0.61 and −0.88 volt. It is clear that the magnitudes of the peaks decrease with GO contents. This indicates that the interface state density is changed with GO content.

4. Conclusions

The electrical and optical properties of Al/GO:C8-BTBT/n-Si/Au diodes were investigated. The diodes exhibit a non-ideal *I–V* behaviour due to the series resistance and interface states properties. The photoconducting mechanism of the diodes is strongly affected by the traps. The diodes exhibit a good photoresponse behavior with low open circuit voltage, low short circuit current and high photocurrent values, confirming its excellent photocurrent response to light intensity. The obtained results suggest that the Al/GO:C8-BTBT/n-Si/Au diodes can be used as a sensor in optoelectronic applications.

Fig. 10. C–V (a), C_{adj}–V (b), G–V (c) and G_{adj}–V (d) characteristics of Al/GO:C8-BTBT/n-Si/Au diode at various frequencies for x=0.6.

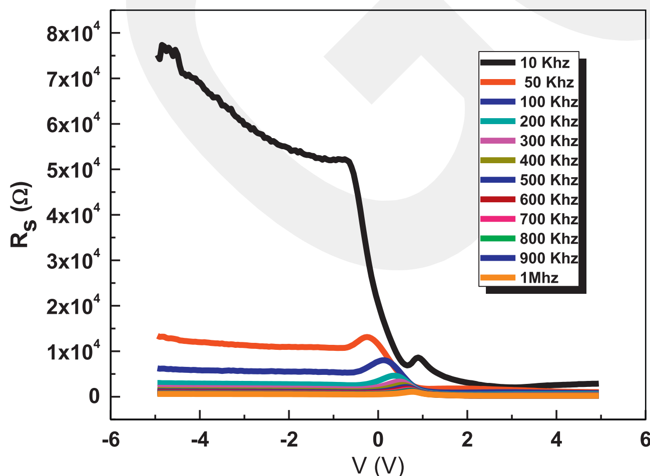

Fig. 11. R_s–V characteristics of Al/GO:C8-BTBT/n-Si/Au diode at various frequencies for $x = 0.6$.

Acknowledgements

The authors gratefully acknowledge and thank the Deanship of Scientific Research, King Abdulaziz University (KAU), Jeddah, Saudi Arabia, for the research group "Advances in composites, Synthesis and applications". This work is as a result of international collaboration of the group with Prof. F. Yakuphanoglu.

H.U. acknowledges support from The Science Academy, Young Scientists Award Program (BAGEP) and AGU-BAP (FOA-2015-24).

References

[1] (a) H. Usta, M.D. Yilmaz, A.J. Avestro, D. Boudinet, M. Denti, W. Zhao, J.F. Stoddart, A. Facchetti, Adv. Mater. 25 (2013) 4327;
(b) H. Usta, W.C. Sheets, M. Denti, G. Generali, R. Capelli, S. Lu, X. Yu, M. Muccini, A. Facchetti, Chem. Mater. 26 (2014) 6542.

[2] C.J. Brabec, N.S. Sariciftci, J.C. Hummelen, Adv. Funct. Mater. 11 (2001) 15.

[3] Kh.S. Karimov, M.M. Ahmed, S.A. Moiz, M.I. Fedorov, Sol. Energy Mater. Sol. Cells 87 (2005) 61.

[4] S.A. Moiz, M.M. Ahmed, Kh.S. Karimov, Jpn. J. Appl. Phys. 44 (2005) 1199.

[5] A. Tapponnier, R.U.A. Khan, C. Marcolli, P. Günter, Thin Solid Films 515 (2007) 3061.

[6] S. Gunes, N.S. Sariciftci, Inorgan. Chim. Acta 361 (2008) 581.

[7] Kh.M. Akhmedov, K.S. Karimov, M.I. Fiodorov, Geliotekhnika 1–3 (1997) 625.

[8] N.A. Davidenko, S.L. Studzinskii, N.A. Derevyanko, A.A. Ischenko, Y.A. Skryshevskii, Semiconductor 36 (2002) 1169.

[9] M.M. Ahmed, Kh.S. Karimov, S.A. Moiz, IEEE Trans. Electron. Devices 51 (2004) 121.
[10] A.V. Kukhta, E.E. Kolesnik, A.I. Lesnikovich, M.N. Nichick, D.V. Ritchik, S.A. Vorobyova, Mater. Sci. Eng. C 26 (2006) 1012.
[11] I.A. Bulgarovskaya, V.M. Vozzhennike, R.M. Gitina, D.V. Pebalk, B.V. Koto, Russ. J. Phys. Chem. 76 (2002) 291.
[12] N.A. Davidenko, L.I. Feneko, N.A. Derevyanko, A.A. Ischenko, M. Kuzma, P.S. Smertenko, S.V. Svechnikov, Synth. Met. 122 (2001) 173.
[13] S.A. Moiz, M.M. Ahmed, Kh.S. Karimov, M. Mehmood, Thin Solid Films 516 (2007) 72.
[14] Hao Chang, Yunfeng Deng, Yanhou Geng, Tong Wang, Donghang Yan, Org. Electron. 22 (2015) 86–91.
[15] Y. Dan, Y. Lu, N.J. Kybert, Z. Luo, A.C. Johnson, Nano Lett. 9 (2009) 1472–1475.
[16] K.I. Bolotin, K. Sikes, Z. Jiang, M. Klima, G. Fudenberg, J. Hone, P. Kim, H. Stormer, Solid State Commun. 146 (2008) 351–355.
[17] A.A. Balandin, S. Ghosh, W. Bao, I. Calizo, D. Teweldebrhan, F. Miao, C.N. Lau, Nano Lett. 8 (2008) 902–907.
[18] M.J. McAllister, J.-L. Li, D.H. Adamson, H.C. Schniepp, A.A. Abdala, J. Liu, M. Herrera-Alonso, D.L. Milius, R. Car, R.K. Prud'homme, Chem. Mater. 19 (2007) 4396–4404.
[19] Bo Wang, Zhimin Chen, Jianan Zhang, Jingjing Cao, Shuxia Wang, Qiuge Tian, Ming Gao, Qun Xu, Colloids Surf. A 457 (2014) 318–325.
[20] B. Košata, V. Kozmik, J. Svoboda, P. Novotaná Vanák, M. Glogarvá, Liq. Cryst. 30 (2003) 603–610.
[21] S.M. Sze, Physics of Semiconductor Device, 2nd ed., John Wiley & Sons, New York, 1981.
[22] A. Astito, A. Foucaran, G. Bastide, M. Rouzeyre, J. Appl. Phys. 70 (1991) 2584.
[23] A. Ahaitouf, E. Losson, A. Bath, Solid-State Electron. 44 (2000) 515.
[24] S.M. Sze, Physics of Semiconductor Devices, John Wiley & Sons, New York, 1981.
[25] C.N. Van, K.P. Kamloth, Thin Solid Films 392 (2001) 113.
[26] M.M. El-Nahass, H.M. Zeyada, M.S. Aziz, N.A. El-Ghamaz, Solid-State Electron. 49 (2005) 1314.
[27] J. Nelson, The Physics of Solar Cells, Imperical College Press, UK, 2003.
[28] R.K. Gupta, R.A. Singh, Mater. Chem. Phys. 86 (2004) 279.
[29] S.S.K. Cheung, N.W. Cheung, Appl. Phys. Lett. 49 (1986) 85.
[30] F. Yakuphanoglu, Y. Caglar, M. Caglar, S. Ilican, Mater. Sci. Semiconductor Process. 13 (2010) 137.
[31] H. Norde, J. Appl. Phys. 50 (1979) 5052.
[32] R.H. Bube, Photoconductivity of Solids, Wiley, New York, 1960.
[33] A. Rose, Concepts in Photoconductivity, Interscience, New York, 1960.
[34] S.M., Sze, Physics Semiconductor Devices, second ed., NewYork, 1981.
[35] W.A. Hill, C.C. Coleman, Solid-State Electron. 23 (1980) 987.
[36] E.H. Nicollian, J.R. Brews, Metal Oxide Semiconductor (MOS) Physics and Technology, Wiley, NewYork, 1982.
[37] E.H. Nicollian, A. Goetzberger, Bell Syst. Tech. J. 46 (1967) 1055.
[38] E.H. Nicollian, A. Goetzberger, Bell Syst. Tech. J. 46 (1967) 1055–1133.
[39] E.H. Nicollian, A. Goetzberger, Appl. Phys. Lett. 7 (1965) 216–219.
[40] E.H. Nicollian, J.R. Brews, MOS Physics and Technology, John Willey & Sons, New York, 1982.
[41] P. Chattopadhyay, B. Raychaudhuri, Solid-State Electron. 35 (1992) 1023.
[42] A. Tataroglu, S. Altındal, Microelectron. Eng. 85 (2008) 2256.
[43] B. Tataroglu, S. Altındal, A. Tataroglu, Microelectron. Eng. 83 (2006) 2021.

GCRIS